Challenge Journal of STRUCTURAL MECHANICS

Research Article

Variations in CFD simulations of wind loading on building structures

Lyubomir A. Zdravkov [a,*]

[a] *Department of Steel, Timber and Plastic Structures, University of Architecture, Civil Engineering and Geodesy (UACEG), Sofia 1046, Bulgaria*

ABSTRACT

Relevant standards for wind loading provide information about wind loads on a small number of standardized building shapes. However, when designing a uniquely shaped structure, two main approaches are possible – either test the structure in a wind tunnel or perform a numerical simulation. With increasing computational power and advances in numerical simulation software, more and more scientific and applied research is being done virtually. Research on fluid flow and the resulting load on machines, industrial facilities and buildings is no exception. In these studies, the first issue is the reliability of the numerical models and, above all, the results obtained through them. Although the programs for numerical simulations have user-friendly interfaces, broad applicability, and advanced solution capabilities, it is not always clear how accurate the results obtained from them are. This article presents a numerical model of a single cylindrical body with a conical roof, subjected to subsonic wind flow. It also shows how, by varying the parameters when creating the model, as the type of finite elements, dimensions of wind tunnel, density of mesh, used RANS model to simulate the turbulence, significant differences can be accounted for in the required computational time and the calculated values of the shear force at its base. It turns out that of all the parameters listed above, the most important is the influence of the dimensions of the finite elements of the fluid domain, i.e., the density of the mesh.

ARTICLE INFO

Article history:
Received – February 26, 2026
Revision requested – April 8, 2026
Revision received – April 19, 2026
Accepted – May 1, 2026

Keywords:
Vertical cylinder
Wind flow
Wind loading
CFD-analysis
RANS model
Mesh density
Finite elements

Citation: Zdravkov LA (2026). Variations in CFD simulations of wind loading on building structures. *Challenge Journal of Structural Mechanics*, 12(2), 115–124.

1. Introduction

Building structures are positioned outdoors and should be designed to withstand the expected wind loads. Relevant standards, such as AS/NZS 1170.2:2021 (2021) and EN 1991-1-4:2005+A1:2010 (2010), provide detailed and relatively user-friendly methods for determining the wind loads on common buildings and structures. Unfortunately, a few standardized shapes are considered in these standards (Xing et al. 2023). However, when it comes to designing a structure that is uniquely shaped, we enter into new, unknown territory. Two main approaches are possible here – to test the structure in a wind tunnel or to perform a numerical simulation. The first choice is well-established and widely adopted, but requires expensive infrastructure and well-trained personnel. Moreover, a study conducted in two different wind tunnels is likely to show noticeable differences in the results obtained, Koss (2000). The second approach is becoming more and more popular due to increased computational power, advances in numerical simulation software and short project timelines. There could be also added full control of input parameters, unlimited access to the details of flow and low cost (Hadane et al. 2023), increasing design flexibility (Abu-Zidan et al. 2020) and easy change of the geometry of the model, where 3D CAD modelling is directly connected with the simulation program (Thordal et al. 2019). And here the question of the

* *Corresponding author*. E-mail address: zdravkov_fce@uacg.bg (L. A. Zdravkov)
ISSN: 2149-8024 / DOI: https://doi.org/10.20528/cjsmec.2026.02.005

reliability of the created numerical simulations and the results obtained through them comes up. Because the programs for numerical simulation have an increasingly friendly interface, their scope of application is growing, and they offer complex solutions, but it is not clear how closely the results represent reality. To help designers in CFD modelling, various documents have been written, such a Japanese "AIJ guide for numerical prediction of wind loads on buildings" (2005). It provides a remarkable number of details regarding the use of computational wind engineering (Xing et al. 2023), but it is a very old document and European standard EN 1991-1-4:2005+A1:2010 (2010) ignores it.

In essence, all numerical simulations are an approximation to the truth, i.e., errors in the results are inevitable. In general, the reasons for this can be:

- Systematic errors in the programs for analysis - they may be embedded in the program code due to ignorance of the physics of the processes being studied and/or poorly written code that fails to fully address the problem;
- Errors due to users - they are mostly caused by ignorance of the capabilities of the programs and incorrect use of them.

User errors are chaotic and unpredictable, so the author will not dwell on them. Here, attention will be paid to the influence of different computational models. The most popular model in CFD analysis is Steady State, where the turbulence of the fluid is simulated using Reynolds-averaged Navier-Stokes (RANS) differential equation. In the study of Ong et al. (2010) was demonstrated the reliability of the standard k–ε model for a flow around a circular cylinder.

In their research, Villalpando et al. (2011) made a comparison between RANS models. They studied airfoil using k–ω, Shear stress Transport (SST), Spalart-Allmaras (SA), Reynold Stress Models (RSM) and Re-Normalization Group (RNG) turbulence models. They found that SA and SST models are more accurate for a certain range of angles of attack. The RSM model is the least appropriate model for this type of problem.

Yagmur et al. (2020) compared RANS (k–ε, k–ω), Large Eddy simulations (LES) and Detached Eddy Simulations (DES) models for the simulation of an unsteady flow around a semi-circular cylinder. In that research LES and DES models have shown more consistent results compared to RANS models.

The author does not claim to be able to detect any systematic errors in the most popular computational models for fluid flow simulations. Rather, he would like to draw attention to the variations in results due to different assumptions when modelling an air flow around a cylindrical body. The present work is focused on the influence of:

- Type used popular RANS model – k–ε, k–ω and SST;
- Type of the element – "tetrahedra" or "hexagonal";
- Density of the mesh and ways to refine it;
- Dimensions of the aerodynamic model used.

2. Description of the Computational Model

The present study was conducted using the ANSYS (2024) software package, which is routinely used at the University of Architecture, Civil Engineering and Geodesy (UACEG), and its Fluid Flow (CFX) module. Using the Workbench graphical interface, a numerical model of a vertical cylinder, resting on the ground, was created. Single or clustered arrangements of cylindrical bodies are common in engineering practice (Amer et al. 2025). Flows around these bodies have been extensively studied, but our knowledge about them remains mostly empirical (Ahmed and Wagner 2012).

The researched body has a conical roof, the height of which is f = 50 mm, see Fig. 1. The diameter of the cylindrical body is d = 1,000 mm, and its height is h = 5,000 mm.

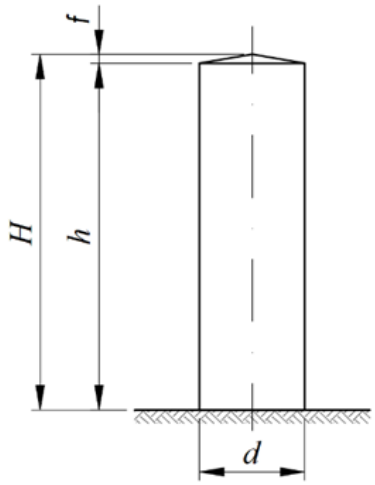

Fig. 1. Shape and dimensions of the researched body.

Around it was created parallelepiped-shaped fluid domains, see Fig. 2. According to Franke et al. (2004, 2007), the walls of the simulated wind tunnels should not be located closer to the researched body than:

- The top/side walls should be placed 5H or more from the obstacle, where H is the total height of the body in the present study ($H = h+f$, see Fig. 1);
- The fluid outlet should be placed at least 15H behind the obstacle.

These distances were derived from earlier studies of Cowan et al. (1997), Hall (1997) and Castro et al. (1999), which were a part of a multi-partner project that evaluated uncertainties in CFD modelling of pollutant dispersion around buildings (Abu-Zidan et al. 2021).

The recommendations of Tominaga et al. (2008) for minimum distances are almost the same as those of Franke et al. (2004, 2007), except for the distance between the obstacle and the fluid outlet. It should be no less than 10H, According to Tominaga et al.

According to Blocken (2015), these distances are sufficient for preventing domain effects in the most computer wind engineering. Revuz et al. (2012) found them very conservative when applied to tall buildings. It is difficult to codify the optimal size of the air domain because it is mainly problem – specific (Abu-Zidan et al. 2021).

The basic dimensions of the fluid domain, accepted by the author, are as follows, see Fig. 2:

- fluid inlet – 30 m;
- fluid outlet – 60 m, i.e., the body is located closer to the entrance of the wind tunnel than to the exit;
- vertical side walls – 30 m;
- "ceiling" of the tunnel – 30 m;
- "bottom" of the tunnel – since in the present simulation the cylindrical bodies are on the ground, the distances between them and the "bottom" are zero.

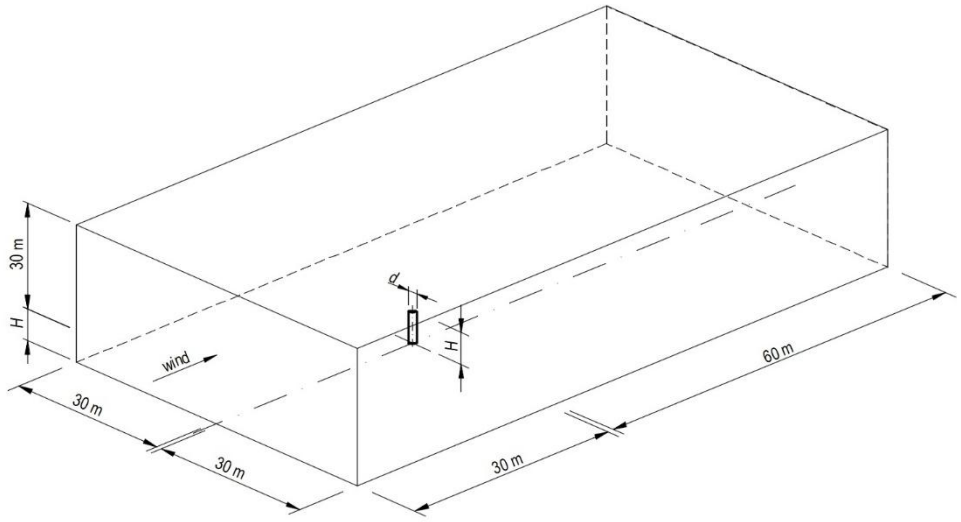

Fig. 2. Shape and dimensions of a basic fluid domain.

The total height of the researched body is $H = h+f =$ 5,050 mm. In other words, the assumed base distances to the tunnel walls are rather $6H$ and $12H$, like the simulations of Hillawaere et al. (2013, 2015). They are much bigger than accepted by Stefanidou et al. (2023) distances $3H$ between the researched body and inlet/outlet/side wall.

Given the above-described restrictions on the minimum distances of the tunnel walls from the researched objects, the main possibility to reduce computational cost and time is to optimize the finite elements mesh. That is, it should be optimised. For this purpose, it should be significantly denser in the area around the facility, and thinned out towards the periphery, as was done in Rusev et al. (2012) and Hui et al. (2023). Here, the author has approached it in two different ways:

a) Fine mesh around the body, without a clearly defined dense zone.

Here, the maximum dimensions of the finite elements of the air around the cylindrical body are limited to:

- elements in direct contact with the cylindrical bodies – 100 mm;
- elements in direct contact with the "bottom" of the tunnel – 500 mm;
- all other elements – 1,000 mm.

b) Fine mesh around the body, with a clearly defined dense zone.

In this approach, a cube is simulated around the body, see Fig. 3, whose walls are located at distances 3, 5 and 8 times the diameter d of the researched body. The maximum dimensions of the finite elements of the fluid are:

- elements in the internal cube, in contact with the cylindrical body – 100 mm;
- the remaining dimensions of the elements are the same as above.

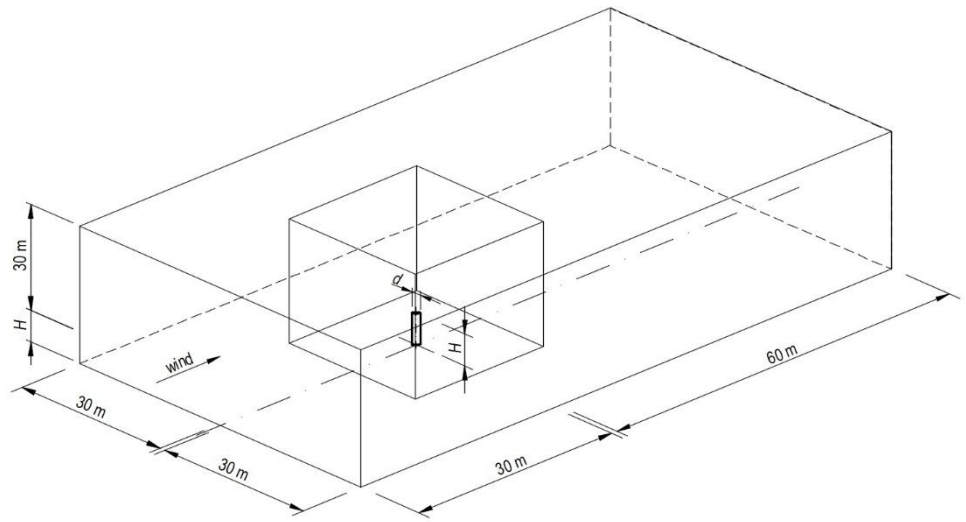

Fig. 3. Shape and dimensions of a basic fluid domain in which a clearly defined zone of fine mesh exists.

The differences in the type of the resulting mesh of elements are shown in Fig. 4.

When creating the mesh of finite elements, the following types of elements were used:

- "Tetrahedra" – pyramidal bodies with a triangular base. Depending on the preservation of the nodes in the middle of their edges, the elements are of type Tet4 (there are no nodes in the middle of the edges,

i.e., 4 nodes per element, see Fig. 5(a)) and type Tet10 (there are nodes in the middle of the edges, i.e., 10 nodes per element, see Fig. 5(b));

- "Hexagonal" – prismatic bodies with a quadrangular base. Depending on the preservation of the nodes in the middle of their edges, the elements are of type Hex8 (there are no nodes in the middle of the edges, i.e., 8 nodes per element, see Fig. 5(c)) and type Hex20 (there are nodes in the middle of the edges, i.e. 20 nodes per element, see Fig. 5(d)).

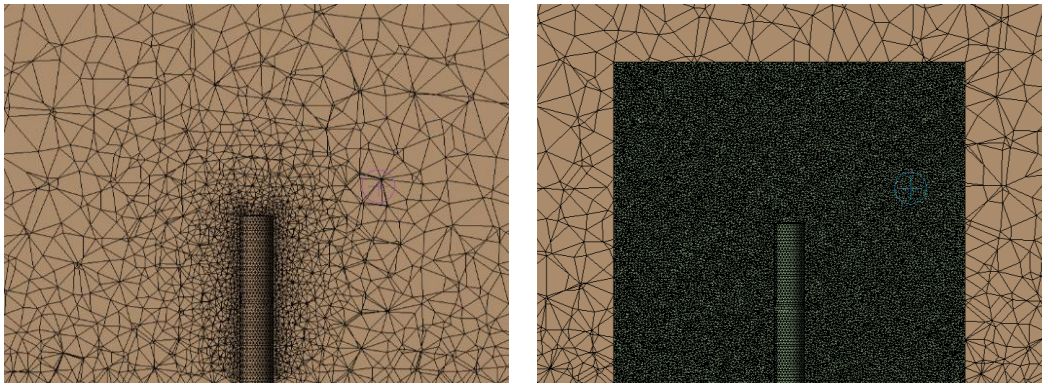

(a) There is no clearly defined zone of fine mesh (b) There exists clearly defined zone of fine mesh

Fig. 4. Ways to change the mesh density around the researched body.

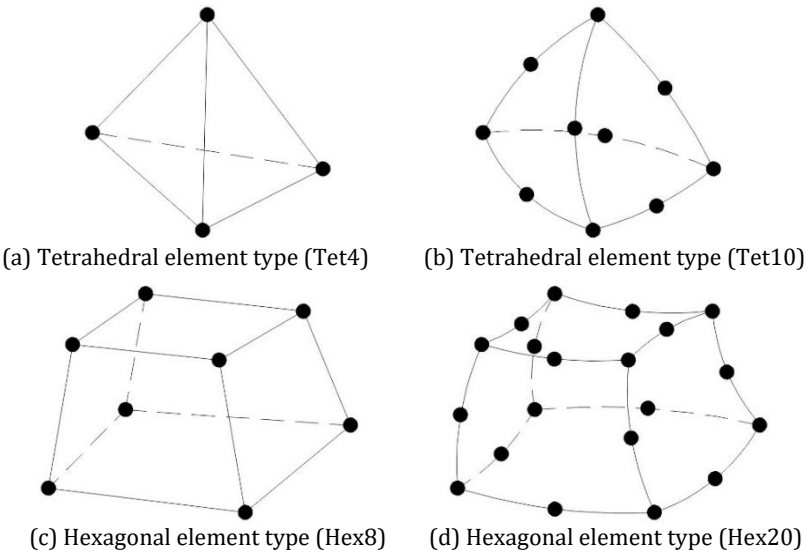

(a) Tetrahedral element type (Tet4) (b) Tetrahedral element type (Tet10)

(c) Hexagonal element type (Hex8) (d) Hexagonal element type (Hex20)

Fig. 5. Finite element types used in the analysis.

The algorithm for creating the mesh of tetrahedra is "patch conforming", i.e., it starts from the edges and surfaces of the bodies. This approach guarantees a "clean" mesh and the is first step to high accuracy of the solution.

Steady State analysis was used in the conducted research. The turbulence of the fluid around the facility was simulated using the well-known Reynolds-averaged Navier-Stokes (RANS) differential equation. According to Agyropulos and Markatos (2015), this equation has the form:

$$\frac{\partial \overline{u_i}}{\partial t} + \frac{\partial (\overline{u_i}\,\overline{u_j})}{\partial x_j} = -\frac{1}{\rho}\frac{\partial \bar{p}}{\partial x_i} + \nu \frac{\partial^2 \overline{u_i}}{\partial^2 x_j} - \frac{\partial \left(\overline{u_i'}\,\overline{u_j'}\right)}{\partial x_j} \tag{1}$$

where $\overline{u_i}$ is the mean speed of the fluid; $\overline{u_i'}$ – the change in the speed of fluid; ρ – the density of the fluid; ν – the cinematic viscosity; t – the time; $\overline{p}$ – the pressure of the fluid; $\overline{u_i'}\,\overline{u_j'} = \tau_{ij}$ – tensor of the stresses of Reynolds.

In analogy to molecular viscous stresses, Reynolds stresses are represented by Markatos (1986) as:

$$\tau_{ij} = \overline{u_i'}\,\overline{u_j'} = \frac{2}{3}k\delta_{ij} - \nu_t\left(\frac{\partial \overline{u_i}}{\partial x_j} + \frac{\partial \overline{u_j}}{\partial x_i}\right) \tag{2}$$

where k is the kinetic turbulence energy. It is calculated by the expression:

$$k = \frac{1}{2}\overline{u_i'}\,\overline{u_i'} = \frac{1}{2}\left(\overline{u_1'^2} + \overline{u_2'^2} + \overline{u_3'^2}\right) \tag{3}$$

$\nu_t = \mu_t/\rho$ – turbulence or eddy (kinematic) viscosity.

Substituting Eq. (2) into Eq. (1), we obtain the expression:

$$\frac{\partial \overline{u_i}}{\partial t} + \frac{\partial (\overline{u_i}\,\overline{u_j})}{\partial x_j} = -\frac{1}{\rho}\frac{\partial \bar{p}}{\partial x_i} + \frac{\partial}{\partial x_j}\left[(\nu + \nu_t)\frac{\partial \overline{u_i}}{\partial x_i}\right] \tag{4}$$

In the models with one equation of transport, ν_t is accounted for by the expression:

$$\nu_t = C_{\nu 1}\sqrt{kL} \tag{5}$$

in which $C_{\nu 1}$ is a dimensionless parameter.

In two-equation models, in addition to the Navier-Stokes equation for the basic (mean) flow, two more transport equations are used, describing two turbulence parameters. This class of models is the most preferred in engineering practice and, according to Hanjalic (2005), is likely to remain so in the near future. Two-equation models are still the first choice for general CFD simulations, where the standard k–ε model of Launder and Sharma (1974) and k–ω of Wilcox (1988) are the most widely used (Agyropulos and Markatos, 2015).

The features of the standard k–ε model of Launder and Sharma (1974) are as follows:

The kinematic eddy viscosity ν_t is calculated by:

$$\nu_t = C_\mu \frac{k^2}{\varepsilon} \tag{6}$$

and turbulence kinetic energy k:

$$\frac{\partial k}{\partial t} + \overline{u_j}\frac{\partial k}{\partial x_j} = \frac{\partial}{\partial x_j}\left[\frac{(\nu+\nu_t)}{\sigma_k}\frac{\partial k}{\partial x_j}\right] - \varepsilon + \tau_{ij}\frac{\partial \overline{u_i}}{\partial x_j} \tag{7}$$

Turbulence dissipation rate ε is determined by the expression:

$$\frac{\partial \varepsilon}{\partial t} + \overline{u_j}\frac{\partial \varepsilon}{\partial x_j} = \frac{\partial}{\partial x_j}\left[\frac{(\nu+\nu_t)}{\sigma_\varepsilon}\frac{\partial \varepsilon}{\partial x_j}\right] - C_{\varepsilon 1}\frac{\varepsilon}{k}\tau_{ij}\frac{\partial \overline{u_i}}{\partial x_j} - C_{\varepsilon 2}\frac{\varepsilon^2}{k} \tag{8}$$

where σ_k = 1.0 and σ_ε = 1.3 are *Prandtl* numbers for k and ε.

The remaining constants for the k–ε model are; C_μ = 0.09; $C_{\varepsilon 1}$ = 1.44 and $C_{\varepsilon 2}$ = 1.92.

The k–ω model was first proposed by Kolmogorov (1941) in 1941. Many researchers have worked on its improvement, with the most significant contribution, according to Agyropulos and Markatos (2015), being Wilcox (1988). There will be present the latest version of Wilcox (2006):

The kinematic eddy viscosity ν_t is calculated by:

$$\nu_t = \frac{k}{\tilde{\omega}} \tag{9}$$

where:

$$\tilde{\omega} = \max\left\{\omega, C_{\lim}\sqrt{\frac{2S_{ij}S_{ij}}{\beta^*}}\right. \tag{10}$$

in which ω is the specific dissipation rate; C_{lim} = 7/8; S_{ij} – tensor of the deformations.

The turbulence kinetic energy k is determined by the expression:

$$\frac{\partial k}{\partial t} + \overline{u_j}\frac{\partial k}{\partial x_j} = \frac{\partial}{\partial x_j}\left[\left(\nu + \sigma^*\frac{k}{\omega}\right)\frac{\partial k}{\partial x_j}\right] - \beta^* k\omega + \tau_{ij}\frac{\partial \overline{u_i}}{\partial x_j} \tag{11}$$

Specific dissipation rate ω:

$$\frac{\partial \omega}{\partial t} + \overline{u_j}\frac{\partial \omega}{\partial x_j} = \frac{\partial}{\partial x_j}\left[\left(\nu + \sigma\frac{k}{\omega}\right)\frac{\partial \omega}{\partial x_j}\right] - \beta\omega^2 + \frac{\sigma_d}{\omega}\frac{\partial k}{\partial x_j}\frac{\partial \omega}{\partial x_j} + a\frac{\omega}{k}\tau_{ij}\frac{\partial \overline{u_i}}{\partial x_j} \tag{12}$$

The coefficients in Eqs. (11) and (12) are: a = 0.52; $\beta = \beta_0 f_\beta$; β_0 = 0.0708; β^* = 0.09; σ = 0.5; σ^* = 0.60; σ_{d0} = 0.125; in which:

$$\sigma_d = \begin{cases} 0, & \frac{\partial k}{\partial x_j}\frac{\partial \omega}{\partial x_j} \le 0 \\ \sigma_{d0}, & \frac{\partial k}{\partial x_j}\frac{\partial \omega}{\partial x_j} > 0 \end{cases} \tag{13}$$

$$f_\beta = \frac{1+85\chi_\omega}{1+100} \tag{14}$$

$$\chi_\omega = \left|\frac{\Omega_{ij}\Omega_{ik}S_{ki}}{(\beta^*\omega)^3}\right| \tag{15}$$

The Shear Stress Transport model (SST) of Menter (1994) is an advanced model for simulating turbulence. This model combines the advantages of the k–ε and k–ω models in predicting aerodynamic flows, and in particular in predicting boundary layers under strong adverse pressure gradients, according to Agyropulos and Markatos (2015).

The k–ε, k–ω and SST models, described above, do not consider the time-dependent flow, which, according to Franke et al. (2007), adequately represents the reality in physical wind tunnels. That is, the results obtained with numerical methods can be directly compared with those measured in real life.

The turbulence intensity was assumed to be 5% average in the research. When the fluid flows around the facility, there are no combustion processes or heat radiation. The air was modelled as an ideal gas with a temperature of 25 °C. Its velocity at the inlet to the enclosure has a value of v = 25 m/s, which is common in continental Europe. The velocity is constant in height because the author is focused on studying the influence of the parameters written above and did not want to further complicate his numerical models. The flow regimes in the areas of the inlet and outlet are subsonic. The relative pressure at the outlet is 0 Pa. This type of boundary condition simulates an open outlet that does not prevent the fluid from leaving the domain (Sun and Zhang, 2025). The flow direction is horizontal and aligned with the longitudinal axis of the wind tunnel. The surfaces of the cylindrical body are fixed walls without roughness. The surface of the terrain around the facility is also smooth, as in the earlier studies of Zdravkov (2022, 2024).

Unlike the research of Mei Yu et al. (2011), the present study considers a horizontal main wind flow, i.e., the angle of attack is 0°.

During its movement, the wind flows around the cylindrical body, see Fig. 6(a), which leads to the appearance of pressure on its elements, see Fig. 6(b). As a result, horizontal forces $F_{h,i}$ are generated at the base of the cylindrical body, which can be easily calculated. It is expected that different numerical modelling assumptions will lead to different horizontal forces. In the present study, it was varied with:

- The model used to simulate turbulence (k–ε, k–ω and SST);
- The dimensions of fluid domains;
- The used finite elements (tetrahedral and hexagonal);
- The finite elements do not have nodes in the middle of the edges (type Tet4 and Hex8) or have them (type Tet10 and Hex20), see Fig. 5;
- The ways of densifying the mesh of elements around the researched body;
- Different density of the mesh.

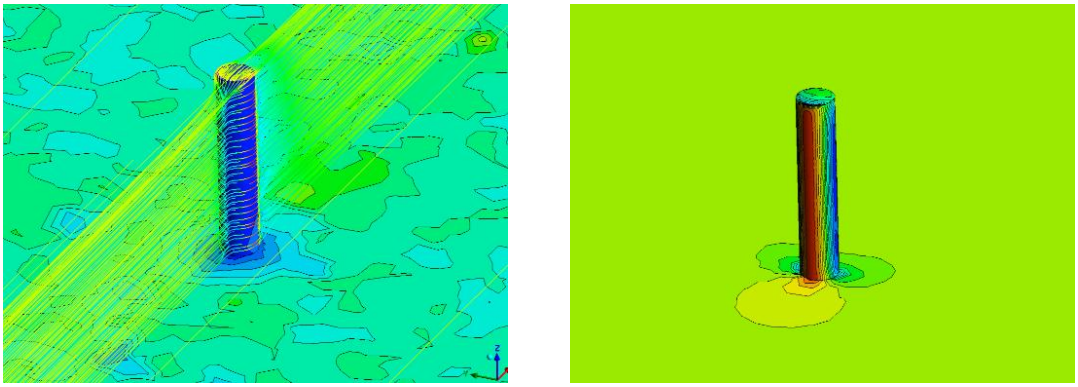

(a) wind flow around the body (b) pressure on body's surface

Fig. 6. Wind flow around the cylindrical body and resultant pressure on its surface.

This research was conducted on a computer with an Intel(R) Core(TM) i7-8700K CPU @ 3.70GHz and 48 GB RAM.

3. Results

By varying the values of the initial parameters described above, we can see how they affect:

- The number of finite elements and nodes, see Table 1;
- The required calculation time, and the horizontal forces in the foundation, see Table 2.

These outcomes reveal that:

- Reduced 50% everywhere fluid domain – the distances between the cylindrical body and the inlet, outlet and side walls are 50% of what is shown in Fig. 3;
- Usual (100% enclosure) fluid domain – the distances between the cylindrical body and the inlet, outlet and side walls are as shown in Fig. 3;
- Elongated 50% after body fluid domain – the distances between the cylindrical body and the inlet and side walls are as shown in Fig. 3. Distance between the body and outlet is elongated with 50%, i.e. 90 m;
- Enlarged (200% enclosure) fluid domain – the distances between the cylindrical body and the inlet, outlet and side walls are twice as large as shown in Fig. 3;
- Enlarged (300% enclosure) fluid domain – the distances between the cylindrical body and the inlet, outlet and side walls are three times larger than shown in Fig. 3;
- Single enclosure – one fluid domain with shape as shown in Fig. 3;
- Double enclosure 3d, 5d and 8d – two fluid domains with shapes as shown in Fig. 4. Distances between the cylindrical body and side walls of internal enclosure are equal to 3, 5 and 8 times the diameter of the body;
- Usual mesh – the maximum dimensions of finite elements are as written above;
- Double denser mesh – the maximum dimensions of finite elements are two times smaller than usual.

Within the framework of the present study, conducted at a relatively low wind speed, the following conclusions can be drawn:

- Numerical models are solved fastest when using k–ω models, and longest – when using SST models;
- There is no significant difference in the values of the shear force $F_{h,i}$ if:
  - k–ε, k–ω or SST models are used to simulate turbulence;
  - the used finite elements have nodes in the middle of their edges (Tet10 and Hex20) or do not (Tet4 and Hex8). However, Tet4 and Hex8 elements save computer time;
  - the dimensions of the wind tunnels are increased in all directions above the values, specified by Tominaga et al. (2008);
  - the wind tunnels are extended to at least 15H after the obstacle, according to the recommendations of Franke et al. (2004, 2007).
- Using Tet4 elements results in lower shear forces compared to models using Hex8 or Hex20 elements, which, according to the author, is more reliable;
- Creating a finer mesh of elements at a distance greater than 5d from the body, see Fig. 3, almost does not change the value of the shear force Fh,i . Only the required calculation time increases;
- Changing the mesh density has the most significant impact on the shear force $F_{h,i}$.

Out of curiosity, the author determined the shear force $F_{h,i}$ at the base of the cylindrical body according to the methodology, described in standard EN 1991-1-4:2005+A1:2010. The analytically determined value is $F_{h,a}$ = 722.6 N. The significant difference between the numerically and analytically determined values of $F_{h,I}$, forced the author to change the most influential factor, the density of the element mesh. He created another numerical simulation with the initial conditions as follows:

- Type of wind tunnel – with a clearly defined zone of fine mesh, as shown in Fig. 3;
- Simulation of turbulence – by means of a k–ω model;
- Finite elements – type Tet4, see Fig. 5(a);
- The elements have the following maximum dimensions:
  - in direct contact with the cylindrical body – 30 mm;
  - in the densification zone around the cylindrical body – 50 mm;
  - along the bottom – 500 mm.

Shear force $F_{h,i}$ = 626.3 N was calculated in this model, i.e. much closer to the analytically determined one.

The author tried to continue in this direction by further lowering the size of the finite elements, but due to insufficient computer memory, ANSYS terminated the calculations.

Table 1. Input parameters when creating numerical models.

Model	Fluid domain		Mesh	Element		Nodes
	Dimensions	Enclosure		Type	Number	Number
k–ε	reduced 50% everywhere	single	usual	Tet4	305539	59268
	usual (100% enclosure)		usual	Tet4	820189	158360
	elongated 50% after body		usual	Tet4	1054378	203469
	enlarged (200% enclosure)		usual	Tet4	3191461	612290
	enlarged (300% enclosure)		usual	Tet4	7262095	1388649
	usual (100% enclosure)		double denser	Tet4	14283270	2480741
	usual (100% enclosure)		usual	Tet10	818091	158015
	usual (100% enclosure)		usual	Hex8	557268	478007
	usual (100% enclosure)		usual	Hex20	594889	528265
k–ω	reduced 50% everywhere	single	usual	Tet4	305539	59268
	usual (100% enclosure)		usual	Tet4	820189	158360
	elongated 50% after body		usual	Tet4	1054378	203469
	enlarged (200% enclosure)		usual	Tet4	3191461	612290
	enlarged (300% enclosure)		usual	Tet4	7262095	1388649
	usual (100% enclosure)		double denser	Tet4	14283270	2480741
	usual (100% enclosure)		usual	Tet10	818091	158015
	usual (100% enclosure)		usual	Hex8	557131	478709
	usual (100% enclosure)		usual	Hex20	594889	528265
SST	reduced 50% everywhere	single	usual	Tet4	305539	59268
	usual (100% enclosure)		usual	Tet4	820189	158360
	elongated 50% after body		usual	Tet4	1054378	203469
	enlarged (200% enclosure)		usual	Tet4	3191461	612290
	enlarged (300% enclosure)		usual	Tet4	7262095	1388649
	usual (100% enclosure)		double denser	Tet4	14283270	248074
	usual (100% enclosure)		usual	Tet10	818091	158015
	usual (100% enclosure)		usual	Hex8	554932	474634
	usual (100% enclosure)		usual	Hex20	617733	547787
k–ε	reduced 50% everywhere	double, 5*d*	external - usual, internal - max 100 mm	Tet4	10351405	1780606
	usual (100% enclosure)	double, 3d		Tet4	4053470	719198
	usual (100% enclosure)	double, 5*d*		Tet4	10937952	1893672
	usual (100% enclosure)	double, 8*d*		Tet4	32387449	5538028
	elongated 50% after body	double, 5*d*		Tet4	11162016	1937008
	enlarged (200% enclosure)	double, 5*d*		Tet4	13314339	2348872
	enlarged (300% enclosure)	double, 5*d*		Tet4	17389209	3126457
	usual (100% enclosure)	double, 5*d*		Tet10	10934940	1893314
	usual (100% enclosure)	double, 5*d*		Hex8	1566889	1349447
	usual (100% enclosure)	double, 5*d*		Hex20	1565995	1347058
k–ω	reduced 50% everywhere	double, 5*d*	external - usual, internal - max 100 mm	Tet4	10351405	1780606
	usual (100% enclosure)	double, 3d		Tet4	4053470	719198
	usual (100% enclosure)	double, 5*d*		Tet4	10937952	1893672
	usual (100% enclosure)	double, 8*d*		Tet4	32387449	5538028
	elongated 50% after body	double, 5*d*		Tet4	11162016	1937008
	enlarged (200% enclosure)	double, 5*d*		Tet4	13314339	2348872
	enlarged (300% enclosure)	double, 5*d*		Tet4	17389209	3126457
	usual (100% enclosure)	double, 5*d*		Tet10	10934940	1893314
	usual (100% enclosure)	double, 5*d*		Hex8	1554627	1340073
	usual (100% enclosure)	double, 5*d*		Hex20	1559627	1341328
SST	reduced 50% everywhere	double, 5*d*	external - usual, internal - max 100 mm	Tet4	10351405	1780606
	usual (100% enclosure)	double, 3d		Tet4	4053470	719198
	usual (100% enclosure)	double, 5*d*		Tet4	10937952	1893672
	usual (100% enclosure)	double, 8*d*		Tet4	32387449	5538028
	elongated 50% after body	double, 5*d*		Tet4	11162016	1937008
	enlarged (200% enclosure)	double, 5*d*		Tet4	13314339	2348872
	enlarged (300% enclosure)	double, 5*d*		Tet4	17389209	3126457
	usual (100% enclosure)	double, 5*d*		Tet10	10934940	1893314
	usual (100% enclosure)	double, 5*d*		Hex8	1572280	1353891
	usual (100% enclosure)	double, 5*d*		Hex20	1562145	1342599

Table 2. Necessary computational time and shear forces in the base of the body.

Model	Fluid domain		Mesh	Element	Time	Force $F_{h,i}$
	Dimensions	Enclosure		Type	Hour	N
k–ε	reduced 50% everywhere	single	usual	Tet4	0:06:50	1556,95
	usual (100% enclosure)		usual	Tet4	0:14:12	1542,94
	elongated 50% after body		usual	Tet4	0:17:12	1545,18
	enlarged (200% enclosure)		usual	Tet4	0:52:40	1528,95
	enlarged (300% enclosure)		usual	Tet4	2:05:47	1516,93
	usual (100% enclosure)		double denser	Tet4	8:15:47	1096,45
	usual (100% enclosure)		usual	Tet10	0:19:28	1542,21
	usual (100% enclosure)		usual	Hex8	0:10:00	1660,83
	usual (100% enclosure)		usual	Hex20	0:10:36	1667,72
k–ω	reduced 50% everywhere	single	usual	Tet4	0:04:08	1549,75
	usual (100% enclosure)		usual	Tet4	0:11:07	1544,53
	elongated 50% after body		usual	Tet4	0:24:08	1547,47
	enlarged (200% enclosure)		usual	Tet4	0:37:28	1537,66
	enlarged (300% enclosure)		usual	Tet4	1:23:20	1534,33
	usual (100% enclosure)		double denser	Tet4	6:28:41	1081,02
	usual (100% enclosure)		usual	Tet10	0:12:10	1539,26
	usual (100% enclosure)		usual	Hex8	0:07:58	1683,32
	usual (100% enclosure)		usual	Hex20	0:09:43	1688,32
SST	reduced 50% everywhere	single	usual	Tet4	0:05:58	1548,39
	usual (100% enclosure)		usual	Tet4	0:10:35	1538,56
	elongated 50% after body		usual	Tet4	0:22:37	1542,41
	enlarged (200% enclosure)		usual	Tet4	1:04:50	1532,61
	enlarged (300% enclosure)		usual	Tet4	1:37:01	1523,14
	usual (100% enclosure)		double denser	Tet4	5:17:29	1081,08
	usual (100% enclosure)		usual	Tet10	0:22:31	1539,06
	usual (100% enclosure)		usual	Hex8	0:11:53	1660,14
	usual (100% enclosure)		usual	Hex20	0:13:59	1655,47
k–ε	reduced 50% everywhere	double, 5*d*	external - usual, internal - max 100 mm	Tet4	2:04:04	1129,91
	usual (100% enclosure)	double, 3*d*		Tet4	1:12:23	1147,54
	usual (100% enclosure)	double, 5*d*		Tet4	3:50:51	1126,63
	usual (100% enclosure)	double, 8*d*		Tet4	9:35:55	1119,05
	elongated 50% after body	double, 5*d*		Tet4	3:18:07	1127,14
	enlarged (200% enclosure)	double, 5*d*		Tet4	3:50:45	1113,99
	enlarged (300% enclosure)	double, 5*d*		Tet4	5:24:56	1103,83
	usual (100% enclosure)	double, 5*d*		Tet10	3:35:00	1126,53
	usual (100% enclosure)	double, 5*d*		Hex8	0:28:07	1526,41
	usual (100% enclosure)	double, 5*d*		Hex20	0:27:12	1527,97
k–ω	reduced 50% everywhere	double, 5*d*	external - usual, internal - max 100 mm	Tet4	1:34:37	1120,15
	usual (100% enclosure)	double, 3*d*		Tet4	0:53:22	1143,8
	usual (100% enclosure)	double, 5*d*		Tet4	1:37:08	1116,3
	usual (100% enclosure)	double, 8*d*		Tet4	5:37:04	1112,37
	elongated 50% after body	double, 5*d*		Tet4	1:34:50	1116,71
	enlarged (200% enclosure)	double, 5*d*		Tet4	1:55:12	1114,46
	enlarged (300% enclosure)	double, 5*d*		Tet4	2:51:25	1110,57
	usual (100% enclosure)	double, 5*d*		Tet10	1:41:39	1120,17
	usual (100% enclosure)	double, 5*d*		Hex8	0:24:03	1545,37
	usual (100% enclosure)	double, 5*d*		Hex20	0:24:07	1548,15
SST	reduced 50% everywhere	double, 5*d*	external - usual, internal - max 100 mm	Tet4	3:19:43	1124,35
	usual (100% enclosure)	double, 3*d*		Tet4	1:31:21	1141,74
	usual (100% enclosure)	double, 5*d*		Tet4	3:32:19	1119,82
	usual (100% enclosure)	double, 8*d*		Tet4	10:24:35	1112,4
	elongated 50% after body	double, 5*d*		Tet4	3:32:04	1120,14
	enlarged (200% enclosure)	double, 5*d*		Tet4	4:20:20	1112,88
	enlarged (300% enclosure)	double, 5*d*		Tet4	2:47:13	1110,57
	usual (100% enclosure)	double, 5*d*		Tet10	3:57:20	1119,84
	usual (100% enclosure)	double, 5*d*		Hex8	0:34:03	1510,38
	usual (100% enclosure)	double, 5*d*		Hex20	0:31:42	1512,1

4. Conclusions

With the increase in calculation power of computers and the improvement of the programs for numerical simulation, more and more research on the effects of wind flow is being done virtually. In these studies, the first question is how reliable the obtained results are. When we have a real wind tunnel, we could easily validate the numerical results. In the most cases, when a physical wind tunnel is not available, we should rely on the good practices developed by researchers who worked before us. In this study, the author has checked:

- How appropriate are the recommendations of Franke et al. (2004, 2007) and Tominaga et al. (2008) for the minimum distances of the walls of wind tunnels from the researched body?
- How can we change the values of the obtained results, by varying the input parameters, such the type of RANS model, the type of finite element and the density of mesh, when creating the numerical simulations?

As a result of the present study, conducted with the parameters described above, the following conclusions could be drawn:

- There is no significant difference in the values of the shear force $F_{h,i}$ if k–ε, k–ω or SST models are used to simulate turbulence;
- The adoption of distances of the walls of the wind tunnels from the blown body, larger than those recommended by Tominaga et al. (2008), has little influence on the values of the obtained results;
- When creating the mesh of finite elements, it is advisable to use element type "Tetrahedra", regardless of whether they will be of type Tet4 or Tet10;
- The least computational time is necessary when using k–ω models, without a significant change in the results;
- The mesh density has the most significant impact on the obtained results.

Acknowledgements

None declared.

Funding

The author received no financial support for the research, authorship, and/or publication of this manuscript.

Conflict of Interest

The authors declares no potential conflicts of interest with respect to the research, authorship, and/or publication of this manuscript.

Data Availability

The datasets generated and/or analyzed during the current study are not publicly available but are available from the corresponding author upon reasonable request.

AI Assistance

No AI-based tools were used in the preparation of this manuscript.

Author Contributions

The author declares sole responsibility for all aspects of the study, including conceptualization, methodology, formal analysis, investigation, data curation, visualization, writing of the original draft, and writing, review, and editing of the manuscript.

REFERENCES

Abu-Zidan Y, Mendis P, Gunawardena T (2020). Impact of atmospheric boundary layer inhomogeneity in CFD simulations of tall buildings. *Heliyon*, 6(7), e04274.

Abu-Zidan Y, Mendis P, Gunawardena T (2021). Optimising the computational domain size in CFD simulations of tall buildings. *Heliyon*, 7(4), e06723.

Agyropulos C, Markatos N (2015). Recent advances on the numerical modelling of turbulent flows. *Applied Mathematical Modelling*, 39, 693-732.

Ahmed N, Wagner D (2012). Vortex shedding and transition frequencies associated with flow around a circular cylinder. *AIAA Journal*, 41(3), 542-544.

AIJ guide for numerical prediction of wind loads on buildings (2005). Architectural Institute of Japan, Tokyo, Japan.

Amer M, Abuelyamen A, Parezanovic V, Alkaabi A, Alameri S, Afgan I (2025). A comprehensive review, CFD and ML analysis of flow around tandem circular cylinders at sub-critical Reynolds numbers. *Journal of Wind Engineering & Industrial Aerodynamics*, 257, 105998.

ANSYS v.2024 R1 (2024). Documentation. Ansys Inc., Canonsburg, PA, USA.

AS/NZS 1170.2:2021 (2021). Structural design actions. Part 2: Wind actions. Australian/New Zealand Standard.

Blocken B (2015). Computational fluid dynamics for urban physics: Importance, scales, possibilities, limitations and ten tips and tricks towards accurate and reliable simulations. *Building and Environment*, 91, 219-245.

Castro I, Cowan I, Robins A (1999). Simulations of flow and dispersion around buildings. *Journal of Aerospace Engineering*, 12(4), 145-160.

Cowan I, Castro I, Robins A (1997). Numerical considerations for simulations of flow and dispersion around buildings. *Journal of Wind Engineering and Industrial Aerodynamics*, 67-68, 535-545.

EN 1991-1-4:2005+A1:2010 (2010). Eurocode 1: Actions on structures. Part 1-4: General actions. Wind actions. European Committee for Standardisation, Brussels, Belgium.

Franke J, Hellsten A, Schlunzen H, Carissimo B, editors (2007). *Best practice guideline for the CFD simulation of flows in the urban environment*. COST Action 732, COST Office, Brussels, Belgium.

Franke J, Hirsch C, Jensen A, Krüs H, Schatzmann M, Westbury P, Miles S, Wisse J, Wright N (2004). Recommendations on the use of CFD in wind engineering. *Proceedings of the International Conference on Urban Wind Engineering and Building Aerodynamics*.

Hadane A, Redford J, Gueguin F, Hafid F, Ghidaglia JM (2023). CFD wind tunnel investigation for wind loading on angle members in lattice tower structures. *Journal of Wind Engineering & Industrial Aerodynamics*, 236, 105397.

Hall R (1997). Application of computational fluid dynamics to near-field atmospheric dispersion. *Atmospheric Dispersion Modelling Liaison Committee Annual Report*, 1996.

Hanjalic K (2005). Will RANS survive LES? A view of perspectives. *Journal of Fluids Engineering*, 127(5), 831-839.

Hillewaere J, Degroote J, Lombaert G, Vierendeels J, Degrande G (2015). Wind-structure interaction simulations of ovalling vibrations in silo groups. *Journal of Fluids and Structures*, 59, 328-350.

Hillewaere J, Degroote J, Rezayat A, Vanlanduit S, Lombaert G, Vierendeels J, Degrande G (2013). Numerical investigation of wind induced ovalling vibrations in silo groups. *Proceedings of the 4th ECCOMAS Thematic Conference on Computational Methods in Structural Dynamics and Earthquake Engineering*, Greece.

Hui Y, Al-Obaidi A, Mari T, Gunasagaran S, Ching M (2023). Investigation of the effect of the wind speed on the aerodynamic and architectural design of tall buildings. *Proceedings of the 18th International Engineering Research Conference (Eureca 2022)*, 2523, 012039.

Kolmogorov A (1941). Equations of turbulent motion in an incompressible fluid. *Doklady Akademii Nauk SSSR*, 30(4), 299-303.

Koss H (2000). Einfluss der Simulation des natürlichen Windes auf die Prognose des Überlastrisikos von Hallentragwerken. *Ph.D. thesis*, Ruhr-University of Bochum, Faculty of Civil Engineering, Germany.

Launder B, Sharma B (1974). Application of the energy dissipation model of turbulence to the calculation of flow near a spinning disk. *Letters in Heat and Mass Transfer*, 1, 131-138.

Markatos N (1986). The mathematical modelling of turbulent flows. *Applied Mathematical Modelling*, 10(3), 190-220.

Menter F (1994). Two-equation eddy-viscosity turbulence models for engineering applications. *AIAA Journal*, 32(8), 1598-1605.

Ong M, Utnes T, Holmedal L, Myrhaug D, Pettersen B (2010). Numerical simulation of flow around a circular cylinder close to a flat seabed at high Reynolds numbers using a k-ε model. *Coastal Engineering*, 57(10), 931-947.

Revuz J, Hargreaves D, Owen J (2012). On the domain size for the steady-state CFD modelling of a tall building. *Wind and Structures*, 15, 313-329.

Rusev I, Dinev D, Tanev T (2012). Numerical study of wind actions on nearby tall buildings. *Proceedings of the International Jubilee Scientific Conference UACEG 2012*, Sofia, Bulgaria, 15-17.

Stefanidou S, Markogiannaki O, Paraskevopoulos E (2023). Parametric analysis and reduced order model of resulting wind loading on structural components through CFD simulations. *ECCOMAS Procedia*, 4523-4531.

Sun Y, Zhang Z (2025). Hydrodynamic interaction in a confined corner: A CFD study of flow and force behaviour around a circular cylinder. *Journal of Engineering and Applied Science*, 72, 68.

Thordal M, Bennetsen J, Koss H (2019). Review for practical application of CFD for the determination of wind load on high-rise buildings. *Journal of Wind Engineering & Industrial Aerodynamics*, 186, 155-168.

Tominaga Y, Mochida A, Yoshie R, Kataoka H, Nozu T, Yoshikawa M, Shirasawa T (2008). AIJ guidelines for practical applications of CFD to pedestrian wind environment around buildings. *Journal of Wind Engineering and Industrial Aerodynamics*, 96(10-11), 1749-1761.

Villalpando F, Reggio M, Ilinca A (2011). Assessment of turbulence models for flow simulation around a wind turbine airfoil. *Modelling and Simulation in Engineering*, 2011, 714146.

Wilcox D (1988). Reassessment of the scale-determining equation for advanced turbulence models. *AIAA Journal*, 26(11), 1299-1310.

Wilcox D (2006). *Turbulence modelling for CFD*. 3rd ed. DCW Industries Inc.

Xing J, Patruno L, Miranda S, Pinardi S, et al. (2023). Early stages wind load assessment using computational fluid dynamics: The new Bologna Stadium roof. *Structures*, 47, 1912-1926.

Yagmur S, Dogan S, Aksoy M, Goktepeli I (2020). Turbulence modelling approaches on unsteady flow structures around a semi-circular cylinder. *Ocean Engineering*, 200, 107051.

Yu M, Liao H, Li M, Ma C, Luo N, Liu M (2011). Study on static wind loading coefficients of suspension bridge, based on CFD simulation and wind tunnel test. *Applied Mechanics and Materials*, 66-68, 334-339.

Zdravkov L (2022). Wind loads on girder bridges. *Challenge Journal of Structural Mechanics*, 8(1), 9-16.

Zdravkov L (2024). Influence of the distance between vertical cylinders positioned in a row on the wind load on them. *Challenge Journal of Structural Mechanics*, 10(3), 101-108.